



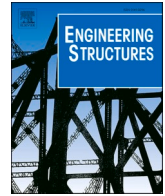
Benchmark of calibrated 2D and 3D track models for simulation of differential settlement in a transition zone using field measurement data

Downloaded from: <https://research.chalmers.se>, 2025-12-04 20:02 UTC

Citation for the original published paper (version of record):

Nasrollahi, K., Ramos, A., Nielsen, J. et al (2024). Benchmark of calibrated 2D and 3D track models for simulation of differential settlement in a transition zone using field measurement data. *Engineering Structures*, 316(2024).
<http://dx.doi.org/10.1016/j.engstruct.2024.118555>

N.B. When citing this work, cite the original published paper.



Benchmark of calibrated 2D and 3D track models for simulation of differential settlement in a transition zone using field measurement data

Kourosh Nasrollahi^{a,*}, Ana Ramos^b, Jens C.O. Nielsen^a, Jelke Dijkstra^c, Magnus Ekh^d

^a Department of Mechanics and Maritime Sciences/CHARMEC, Chalmers University of Technology, SE-412 96 Gothenburg, Sweden

^b CONSTRUCT – LESE, Faculty of Engineering, University of Porto, Portugal

^c Department of Architecture and Civil Engineering, Chalmers University of Technology, Sweden

^d Department of Industrial and Materials Science, Chalmers University of Technology, Sweden

ARTICLE INFO

Keywords:

Transition zone
Differential settlement
Dynamic vehicle–track interaction
2D and 3D models
Calibration

ABSTRACT

Two models for time-domain simulation of vertical dynamic vehicle–track interaction and prediction of differential settlement in a transition zone between a ballasted track and a Moulded Modular Multi-Blocks (3MB) slab track are calibrated and verified using field measurements from a test site on the Swedish iron ore line. The dynamic analysis is performed using two-dimensional (2D) and three-dimensional (3D) track models in MATLAB and ANSYS, respectively. A seven-parameter representation of the ballast and subgrade is applied in the 2D model. It considers sleeper coupling through the ground via a discretised mass-spring-damper system. The more extensive 3D model includes a solid finite element (FE) model of the layered soil foundation with properties determined from a multichannel analysis of surface waves (MASW) carried out at the test site, and with perfectly matching layers (PML) added at the boundaries. The measured responses include rail receptance functions from both track forms on either side of the transition, as well as transient responses in terms of sleeper displacements and rail bending moments generated by the passing heavy-haul traffic. Both models are employed to simulate the passage of an iron ore freight vehicle through the transition zone. The accumulated settlement for one year of traffic is predicted using an iterative approach and compared with the measured long-term sleeper settlement. Good agreement is observed between the measurements and the settlements forecasted by both models, with the simulation time being approximately 25 times shorter for the 2D model.

1. Introduction

In transition zones between two different track forms, there is a discontinuity in track structure leading to a gradient in track stiffness [1–15]. Examples include transitions between different superstructures, such as slab track to ballasted track, and/or between different substructures, like embankment to a bridge or tunnel structure. Differences in loading and support conditions at the interfaces between track superstructure and substructure on either side of the transition may lead to differential track settlement and an irregularity in longitudinal rail level soon after track construction. This results in an amplification of the dynamic traffic loading along the transition, contributing to the degradation process of ballast and subgrade and resulting in a further deterioration of vertical track geometry. Hence, track adjacent to a transition is prone to deteriorate at an accelerating rate, and frequent maintenance work may be required. In recent years, infrastructure managers and

researchers have dedicated increasing attention to life cycle analysis and optimisation of the long-term performance of transition zones using both simulation models and field measurements [16].

Various models have been applied to simulate the dynamic vehicle–track interaction and differential settlement in transition zones. The reliability and accuracy of these analyses are influenced by the complexity of the model. Aspects such as static or dynamic analysis, linear or non-linear analysis (involving irreversible deformations and voided sleepers), computational cost, and desired outputs need to be considered. Comprehensive assessments of models for dynamic vehicle–track interaction in transition zones and their applications were carried out in [8,17]. However, few models have been calibrated and validated versus field measurements. In this study, one two-dimensional (2D) and one three-dimensional (3D) FE model of a transition zone will be calibrated and verified versus measured data [1,9,18].

* Corresponding author.

E-mail address: kourosh.nasrollahi@chalmers.se (K. Nasrollahi).

<https://doi.org/10.1016/j.engstruct.2024.118555>

Received 30 March 2024; Received in revised form 2 June 2024; Accepted 1 July 2024

Available online 10 July 2024

0141-0296/© 2024 The Author(s). Published by Elsevier Ltd. This is an open access article under the CC BY license (<http://creativecommons.org/licenses/by/4.0/>).

The 2D model represents an extended version of the non-linear FE model presented by Nasrollahi et al. [1]. It is used for the simulation of long-term differential track settlement, voided sleeper development, rail seat load redistribution, and evolving irregularities in vertical track geometry during a transition between two track forms. It predicts the accumulated settlement for a specified traffic load using an iterative approach. In this paper, this model is extended to consider the interaction between sleepers via the ground, similar to the model presented by Zhai et al. [19]. The 3D model by Ramos et al. [9] considers short- and long-term behaviour of ballasted and slab tracks subjected to cyclic loading, where the settlement of both types of track form have been verified using laboratory experiments. In [9], the 3D FE model, integrated with an empirical settlement model, was used to analyse a transition zone between a slab track on an embankment and a slab track in a tunnel.

Based on impact load excitation, frequency response functions (FRFs) of track responses provide information on the dynamic properties along a railway structure, such as the inertia, stiffness and damping of various components, offering a comprehensive quantification of the overall system behaviour [20]. However, in most cases, such measurements are carried out for a track without considering a relevant static pre-load. In [21], FRFs measured on a slab track were compared with the corresponding calculated FRFs from both waveguide (2.5D) and 3D FE models. In [22], parameters of the substructure and superstructure in a 2D model of ballasted track were tuned against a periodic finite element-boundary element model. An alternative method for model calibration involves assessing measured dynamic responses from passing traffic. The significant advantage of this approach lies in its ability to better capture the nonlinear response of the track structure in loaded conditions. In [6], pass-by simulations of carbody acceleration, sleeper acceleration, and rail displacement calculated with a 3D FE model of a transition zone were compared with field measurements.

In principle, the deterioration of the longitudinal level of ballasted track can be described as occurring in two phases. Initially, immediately after track construction, there is a rapid deterioration of longitudinal level due to ballast compaction. Subsequently, in the second phase, the deterioration rate (time derivative of the settlements) slows down, primarily leading to a linear increase of settlement with the number of load cycles. During this phase, there is further compaction in the substructure due to the rearrangement and breakdown of ballast caused by fracture and abrasive wear of individual particles. Additional contributing factors are penetration of sub-ballast and sub-grade into ballast voids, along with the inelastic recovery of the sub-grade after unloading. A review of empirical models for soil settlement is presented in [23]. According to numerous empirical formulas derived from laboratory or field measurements, settlement typically follows a logarithmic or power law relationship with the number of axle passes, as outlined in [24].

In the context of long-term track settlement modelling, recent developments have seen the incorporation of empirical methods within an iterative framework. For example, Nasrollahi et al. [1] integrated a 2D vertical dynamic vehicle-track interaction model for the calculation of sleeper-ballast contact forces in the short term with an empirical visco-plastic material mechanics model for the prediction of long-term ballast settlement. Wang and Markine [10] coupled a FE model of the vertical dynamic vehicle-track interaction in a transition zone with an empirical equation inspired by Sato's empirical formula [25] to predict the settlement over 60,000 load cycles. This paper adopts a similar empirical settlement model to predict long-term sleeper settlement as the one introduced in [1], but here the model is calibrated using measured sleeper settlement data from [18]. Rheological models of track settlement have been proposed by Ognibene et al. [26] and Punetha et al. [27]. These models simulate the response of the track substructure layers using equivalent springs, spring-dashpots, homogeneous or multilayered half-spaces, or combinations thereof. Further, a plastic-hardening unit where the hardening parameters are set to increase exponentially with accumulated plastic settlement due to

densification and lateral spreading of the ballast has been implemented. Additionally, a few studies have represented the substructure layers as assemblies of discrete particles. For example, Suiker et al. [28] modelled the ballast as discrete particles connected by elastic longitudinal and shear springs to examine body wave propagation and the steady-state response to a moving, harmonically vibrating load.

In 2022–2023, an extensive field measurement campaign was carried out in a transition zone at *Gransjö* on the Swedish heavy-haul line *Malmbanan* [18]. The transition zone was between a conventional ballasted track and a 3MB slab track. A fibre Bragg grating-based (FBG) long-term monitoring arrangement, with a high temporal resolution, was used for both short-term and long-term condition monitoring of the operational railway track in the harsh conditions in the north of Sweden. The test set-up was limited to measurement of track response and sleeper settlement in four selected sleeper bays. Based on these measured results, this paper calibrates and validates the 2D and 3D track models for time-domain simulation of vertical dynamic vehicle-track interaction, as well as the applied empirical equations to predict differential long-term settlement of sleepers in a transition zone. Measured FRFs (displacement over applied force) are used to tune the input data for the two track models. For a loaded iron ore vehicle passing the transition zone at speed 60 km/h, calculated rail bending moments and sleeper vertical displacements are compared with the corresponding measured responses. For two selected sleepers, the predicted settlements are compared with the corresponding long-term measurements.

The novel contribution of this paper is the critical assessment and comparison of two track models versus extensive field measurements. The aim is to investigate whether a 2D track model with a discretised seven-parameter substructure model is sufficient to predict long-term settlement, or whether the second model with an extensive 3D FEM-PML representation of the transition zone with the superstructure, ballast, and layered soil being represented by solid finite elements is required. The computational cost for the 2D model is significantly lower than for the 3D model at the expense of a much more simplified representation of the foundation. Note that additional substructure layers could have been included in the 2D track model, cf. [27]. However, in this study, this has been neglected since the results from a multi-channel analysis of surface waves (MASW) carried out at the test site indicated very stiff layers of the subgrade [18].

2. Simulation models

In this section, the two track models used in the time-domain simulations of vertical dynamic vehicle-track interaction in a transition zone are described and compared. The models are integrated with empirical equations to calculate the differential settlement along the ballasted side of the transition zone. For a prescribed traffic load, the accumulated long-term settlement is predicted using an iterative approach, where the support conditions of the track model are updated in each iteration step. The first track model is an extended version of the 2D model presented in [1], while the second model is the 3D model that was introduced in [29].

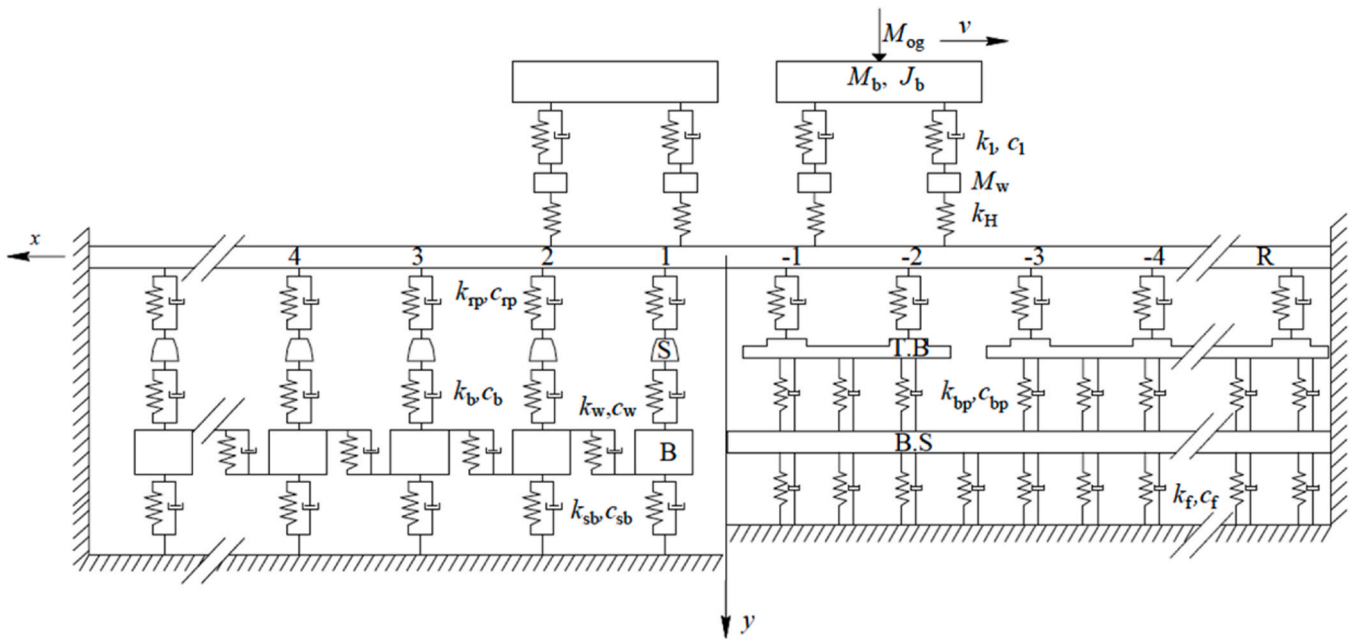
2.1. Two-dimensional (2D) model

2.1.1. Track model

The first model is a reduced-order 2D representation of the transition zone at the test site, see Fig. 1, incorporating a discretised mass-spring-damper system for the interaction between adjacent sleepers through the ground. Symmetric loading with respect to a vertical plane along the track centre is assumed leading to that only half of the track (and vehicle) is considered. The track model accounts for the variation and redistribution of loads supporting adjacent sleepers that occur over time due to accumulated settlement and the potential development of voided sleepers. It considers gravity loads on the track structure, state-dependent track conditions, and (although not considered in the



(a)



(b)

Fig. 1. (a) An overview of the test site including a transition zone between ballasted track and 3MB slab track at Gransjö, north of Boden, Sweden. (b) Sketch of complete 2D vehicle and transition zone model. The track model contains rail (R), top blocks (T.B) and base slab (B.S) modelled by beam elements. The base slab is supported by a Winkler foundation. The sleepers (S) are rigid masses supported by a seven-parameter model of the substructure using non-linear, and potentially random, properties. The ballast (B) mass is part of the substructure model.

present paper) any prescribed variation of non-linear stiffness in the supporting foundation along the track. A time-domain model of vertical dynamic vehicle–track interaction is applied to calculate the contact forces between sleepers and ballast in the short term, cf. Fig. 1(b) and Section 2.1.3. Using an iterative approach, these forces are used as input in an empirical model to determine the increment in ballast/subgrade settlement below each sleeper per vehicle pass-by, see Section 2.1.4.

The track model uses Euler-Bernoulli beam elements for the rail, and for the top blocks and base in the slab track. The properties of the substructure are described by a discretised seven-parameter model. The seven parameters include the mass of the ballast (m_b), a state-dependent discrete spring with stiffness (k_b) and a viscous damper with damping (c_b) representing the combined properties of the ballast layer and under

sleeper pads (USPs), and a shear stiffness (k_w) and shear damping (c_w) to mimic the coupling of the interlocking ballast granules between adjacent ballast masses. Further, the properties of all layers of the subgrade are given by the stiffness (k_{sb}) and the damping (c_{sb}). In each iteration step, the bi-linear stiffness characteristics of k_b are updated to account for a potentially evolving voided distance between sleeper and ballast where the stiffness is zero. For the ballasted track, the seven properties of the subgrade model will be tuned versus the measured rail receptance, see Section 4.

The complete transition zone model has a total length of 48 m (28.8 m of ballasted track and 18.0 m of 3MB slab track) with rigid boundaries at the rail ends. The superstructure of the ballasted track comprises 60 kg/m rails, rubber rail pads, and concrete sleepers

designed for axle loads up to 35 tonnes. The rail is modelled with four beam elements per sleeper bay with bending stiffness ($EI_r = 6.4 \text{ MNm}^2$) and mass per unit length ($m_r = 60 \text{ kg/m}$), while each rail pad is represented by a linear spring-damper element. Each sleeper in the ballasted track is modelled by a discrete (rigid) element with one vertical degree-of-freedom (dof) and mass $m_s = 150 \text{ kg}$. In this paper, sleeper distances L are assumed to be uniform on both the ballasted and slab sides, but this is not a requirement of the model. The sleepers in the ballasted track are numbered with index i ($i = 1, 2, \dots, N_{\text{bays}}-1$; $i > 0$) starting from the transition, cf. Fig. 1(b).

The 3MB concept is a reinforced standard precast slab design that strives to achieve fast and easy maintainability using replaceable, pre-cast components. It is constructed using 4.8 m long modules, each featuring a base slab consisting of two longitudinal reinforced concrete beams connected by two transversal beams. Additionally, there are eight precast moulded concrete blocks, four on each base slab. Vibration isolation and prevention of block hammering against the base slab are achieved by elastomeric strips (block pads) at the interfaces [1,18]. The rail seats in the slab track are numbered with index i ($i = -1, -2, -3, \dots$; $i < 0$), cf. Fig. 1(b). The two-layer slab track is modelled by one continuous beam representing the base slab below a layer of non-interacting beams representing the discrete blocks. Rail properties are labelled with index 'R'. The two layers of the 3MB slab track are labelled 'T.B' and 'B.S', respectively. Each layer of Euler-Bernoulli beam elements has bending stiffness EI and mass m per unit beam length, width b and height h . The vertical connection between each pair of adjacent nodes in the different layers is modelled as a spring and viscous damper in parallel.

Input data for the track model is listed in Table 1. Some input data to the track model, such as the properties of rail, sleepers, top blocks, and base slab, were collected from the literature or provided manuals. However, certain properties were unknown and required calibration, see Section 4. The influence of crib ballast (non-compacted ballast on the surface between two adjacent sleepers) is not considered in the model.

2.1.2. Iterative procedure

As indicated above, the simulation model employs an iterative approach, integrating a time-domain model of vertical dynamic vehicle-track interaction in the short term (accounting for voided sleepers and state-dependent properties of the ballast and subgrade at each sleeper-ballast interface) with an empirical model of accumulated ballast and subgrade settlement in the long term [1,30]. As illustrated in

Fig. 2, the simulation procedure involves performing one time-domain simulation of short-term vehicle-track dynamics in each iteration step. The pre-calculated static track displacement due to gravity load is used as initial conditions to the simulation of vertical dynamic vehicle-track interaction. The calculated load maxima at the interface between each sleeper and ballast in the ballasted track section, generated by the combination of gravity load on the track superstructure and each of the passing wheels of the vehicle model, are used as input to an empirical settlement model. In each iteration step and for each individual sleeper in the track model, the bi-linear properties of the spring stiffnesses k_b of the track model are updated to account for the current states of the support conditions, and it is assumed that the same set of load maxima is generated by all passing vehicles. By taking several iteration steps, the accumulated differential settlement in the long-term, the potential development of voided sleepers and the resulting redistribution of foundation loads between adjacent sleepers are calculated [1].

2.1.3. Vertical dynamic vehicle-track interaction

In this study, where the track model is non-linear, the simulation of vertical dynamic vehicle-track interaction is performed by a direct integration in the time domain. A summary of the procedure is given here. For more details, see [1]. An extended (mixed) state-space vector $\mathbf{z}(t)$ is introduced as

$$\mathbf{z}(t) = \left\{ \mathbf{x}^{t,T} \quad \dot{\mathbf{x}}^{t,T} \quad \mathbf{x}_a^{v,T} \quad \mathbf{x}_b^{v,T} \quad \dot{\mathbf{x}}_a^{v,T} \quad \dot{\mathbf{x}}_b^{v,T} \quad \hat{\mathbf{F}}_a^T(t) \right\} \quad (1)$$

It includes the displacements \mathbf{x}^t and velocities $\dot{\mathbf{x}}^t$ of the transition zone track model. The vertical displacements and velocities of four massless dofs of the vehicle model, cf. Fig. 1(b), that are interfacing the rail are collected in the 4×1 vectors $\mathbf{x}_a^{v,T}$ and $\dot{\mathbf{x}}_a^{v,T}$, respectively, while $\mathbf{x}_b^{v,T}$ and $\dot{\mathbf{x}}_b^{v,T}$ are two 8×1 vectors containing the vertical displacements and velocities of the non-interfacial vehicle dofs, representing the motion of two adjacent bogies in two adjacent iron ore wagons. Further, it contains the impulses $\hat{\mathbf{F}}_a(t) = \int \mathbf{F}_{w/r}(t) dt$ of the wheel-rail contact forces. All equations of motion for vehicle and track, and the algebraic constraint equations coupling the vehicle and track, are assembled in one first-order matrix form as

$$\mathbf{A}(\mathbf{z}, t)\dot{\mathbf{z}} + \mathbf{B}(\mathbf{z}, t)\mathbf{z} = \mathbf{F}(\mathbf{z}, t) \quad (2)$$

with

Table 1

Parameters of the 2D track model. Input data to variable names marked with an asterisk (*) have been determined based on the calibration versus measured rail receptances carried out in Section 4.

Ballasted track side				Slab track side			
	Parameter	Unit	Value		Parameter	Unit	Value
Ballast	Stiffness (k_b) *	MN/m	75	Base slab	Bending stiffness ($EI_{B,S}$)	MNm ²	23.45
	Damping (c_b) *	kNs/m	30		Mass per unit length ($m_{B,S}$)	kg/m	375
	Mass (m_b) *	kg	300		Width ($b_{B,S}$)	m	0.6
	Shear stiffness (k_w) *	MN/m	120		Height ($h_{B,S}$)	m	0.25
	Shear damping (c_w) *	kNs/m	90	Top block	Bending stiffness ($EI_{T,B}$)	MNm ²	11
Subgrade	Stiffness (k_{sb}) *	MN/m	40		Mass per unit length ($m_{T,B}$)	kg/m	275
	Damping (c_{sb}) *	kNs/m	160		Width ($b_{T,B}$)	m	0.55
USP					Height ($h_{T,B}$)	m	0.2
	Stiffness (k_{USP})	MN/m	176	Block pad	Stiffness (k_{bp})	GN/m ³	0.17
	Damping (c_{USP})	kNs/m	120		Damping (c_{bp})	kNs/m	50
	Elasticity modulus	MPa	7.5		Elasticity modulus	Mpa	3.9
	Mass density	kg/m ³	300		Mass density	kg/m ³	300
	Height	mm	15	Rail pad	Height	mm	12.5
	Cross-sectional area	m ²	0.34		Cross-sectional area	m ²	0.55
	Poisson's ratio	-	0.1		Poisson's ratio	-	0.1
Rail pad	Stiffness (k_{rp}) *	MN/m	110		Stiffness ($k_{r/T,B}$)	MN/m	20
	Damping (c_{rp}) *	kNs/m	15	Foundation	Damping ($c_{r/T,B}$)	kNs/m	10
					Stiffness (k_f)	MN/m	10
					Damping (c_f)	kNs/m	10

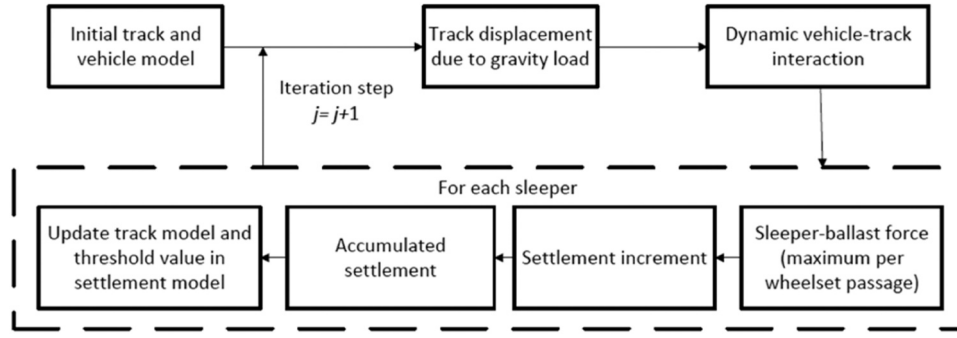


Fig. 2. Iterative procedure to predict differential settlement in a transition zone using the 2D simulation model [1].

$$\mathbf{A}(\mathbf{z}, t) = \begin{bmatrix} \mathbf{0} & \mathbf{M}^t & \mathbf{0} & \mathbf{0} & \mathbf{0} & \mathbf{0} & -\mathbf{N}^T \\ \mathbf{I} & \mathbf{0} & \mathbf{0} & \mathbf{0} & \mathbf{0} & \mathbf{0} & \mathbf{0} \\ \mathbf{0} & \mathbf{I} & \mathbf{0} & \mathbf{0} & \mathbf{0} & \mathbf{0} & \mathbf{I} \\ \mathbf{0} & \mathbf{0} & \mathbf{0} & \mathbf{0} & \mathbf{0} & \mathbf{M}_{bb}^v & \mathbf{0} \\ \mathbf{0} & \mathbf{0} & \mathbf{0} & \mathbf{I} & \mathbf{0} & \mathbf{0} & \mathbf{0} \\ \mathbf{T} & \mathbf{0} & \mathbf{0} & \mathbf{0} & -\mathbf{I} & \mathbf{0} & \mathbf{0} \\ \mathbf{R} & \mathbf{T} & -\mathbf{I} & \mathbf{0} & \mathbf{0} & \mathbf{0} & \mathbf{0} \end{bmatrix} \quad (3)$$

$$\mathbf{B}(\mathbf{z}, t) = \begin{bmatrix} \mathbf{K}^t & \mathbf{C}^t & \mathbf{0} & \mathbf{0} & \mathbf{0} & \mathbf{0} & \mathbf{0} \\ \mathbf{0} & -\mathbf{I} & \mathbf{0} & \mathbf{0} & \mathbf{0} & \mathbf{0} & \mathbf{0} \\ \mathbf{0} & \mathbf{0} & \mathbf{K}_{aa}^v & \mathbf{K}_{ab}^v & \mathbf{0} & \mathbf{0} & \mathbf{I} \\ \mathbf{0} & \mathbf{0} & \mathbf{K}_{ba}^v & \mathbf{K}_{bb}^v & \mathbf{0} & \mathbf{C}_{bb}^v & \mathbf{0} \\ \mathbf{0} & \mathbf{0} & \mathbf{0} & \mathbf{0} & \mathbf{0} & -\mathbf{I} & \mathbf{0} \\ \mathbf{U} & \mathbf{0} & \mathbf{0} & \mathbf{0} & \mathbf{0} & \mathbf{0} & \mathbf{0} \\ \mathbf{S} & \mathbf{0} & \mathbf{0} & \mathbf{0} & \mathbf{0} & \mathbf{0} & \mathbf{0} \end{bmatrix} \quad (4)$$

Here \mathbf{M}^t , \mathbf{K}^t , and \mathbf{C}^t are the mass matrix, stiffness matrix and viscous damping matrix of the track model, whereas \mathbf{K}^v , \mathbf{M}^v and \mathbf{C}^v are the corresponding matrices for the vehicle model. Each wheel–rail contact force is distributed as consistent forces and moments on the adjacent rail nodes using Hermitian interpolation polynomials. By assuming a prescribed vehicle speed $v(t)$ and considering the Coriolis and centripetal accelerations that occur because the vehicle model is moving along the track model, the constraints on the interfacial velocities and accelerations for the massless dofs of the vehicle model are expressed in \mathbf{T} , \mathbf{S} , \mathbf{U} , and \mathbf{R} , cf. [1]. The mixed force vector \mathbf{F} is written as

$$\mathbf{F}(\mathbf{z}, t) = \{\mathbf{F}_{s/b}^{t,T}(t) + \mathbf{F}_g^{t,T} \mathbf{0}^T \mathbf{0}^T \mathbf{F}_b^{v,T}(t) \mathbf{0}^T \mathbf{x}^{irr} \mathbf{x}^{irr}\}^T \quad (5)$$

where the vector $\mathbf{F}_{s/b}^t$ contains the state-dependent contribution to the sleeper–ballast force acting on each sleeper in the ballasted track section (note that any stiffness of the bi-linear spring k_b up to the breakpoint representing the voided distance between sleeper and ballast is considered in \mathbf{K}^t), while the constant vector \mathbf{F}_g^t includes the gravity load on the track superstructure. Further, prescribed external loads (vehicle gravity loads) are assembled in \mathbf{F}_b^v , while \mathbf{x}^{irr} contains the prescribed wheel/rail surface irregularities. It is acknowledged that the wheels passing the transition zone have irregularities ranging from eccentricity with a wavelength in the order of 3 m down to acoustic roughness with wavelengths in the order of centimetres. However, wheel irregularities were not measured in the field test [18]. The track longitudinal level was aligned before the measurements commenced. It is assumed that the influence of the additional dynamic loading due to wheel out-of-roundness, as well as from any initial track irregularity from before the first load cycle, on the accumulated settlement is

negligible compared to the influence from the quasi-static loading caused by the passing wheelsets with axle loads of around 30 tonnes.

The initial value problem for the solution of the transient vibration problem is written as

$$\dot{\mathbf{z}} = \mathbf{A}^{-1}(\mathbf{F} - \mathbf{B}\mathbf{z}), \quad \mathbf{z}(t=0) = \mathbf{z}_0 \quad (6)$$

where \mathbf{z}_0 includes the initial state due to the weight of the track, cf. Fig. 2. In the present study, the solution is obtained using MATLAB's moderately stiff differential equation solver ode23s with an adaptive time step.

2.1.4. Settlement model

The aim of the iterative procedure, see Fig. 2, is to calculate the long-term accumulated differential settlement and track geometry degradation for a given traffic load corresponding to a given number of load cycles (wheel passes). In this paper, an empirical equation inspired by Sato's empirical relationship [23] and the modelling of visco-plastic material mechanics is used to predict the long-term settlement of sleepers. In each iteration step, after solving the short-term vehicle–track interaction problem in the time domain, the time history of each sleeper–ballast force $F_{s/b,i}(t)$ is calculated in a post-processing step using the FE model of the track. For each vehicle model passage in iteration step j ($j = 1, 2, \dots, n_s$), the incremental settlement $\delta_{i,j}$ [m] at sleeper i ($i = 1, 2, \dots, N_{bays}-1$) is formulated as a function of the maximum of the sleeper–ballast–contact force, $\max(F_{s/b,i})$, generated by each passing wheel n .

$$\delta_{i,j} = \sum_{n=1}^{N_w} \left\{ \sum_{k=1}^{N_k} \alpha_k \left[\frac{\langle \max(F_{s/b,i})_n - F_{th,i} \rangle}{F_0} \right]^{\beta_k} \right\} \quad (7)$$

where N_w is the number of wheels in the vehicle model (here, $N_w = 4$). Within each iteration step, it is assumed that the set of $\max(F_{s/b,i})$ remains the same for all vehicle passes such that a linear extrapolation of each settlement increment representing up to 10^5 load cycles can be carried out. The order N_k of the polynomial formulation and the corresponding parameters α_k and β_k are empirical, while $F_0 = 1$ kN is a reference contact force with a unit such that the term within the square brackets becomes non-dimensional. In this settlement model, there is no accumulation of permanent ballast/subgrade deformation if the maximum sleeper–ballast contact force generated by a passing wheel is below a certain threshold value $F_{th,i}$, as reflected in Eq. (7) by the Macaulay brackets. It is assumed that the model provides the permanent deformation accounting for all the layers of the substructure.

The accumulated settlement at sleeper i after n_s iteration steps (corresponding to N_s wheel passes) is calculated by summing the incremental settlements calculated for each preceding step j

$$\Delta_i(n_s) = \sum_{j=1}^{n_s} \delta_{i,j} \quad (8)$$

In the next iteration step, these accumulated settlements are applied in the updated track model. For each sleeper i , it is assumed that the current threshold value $F_{th,i}$ is dependent on the accumulated settlement Δ_i as

$$F_{th,i}(\Delta_i) = F_{th,\infty} - (F_{th,\infty} - F_{th,0})e^{-\gamma\Delta_i} \quad (9)$$

Here $F_{th,0}$ is the virgin threshold value before any traffic loading has been applied, $F_{th,\infty}$ is the long-term threshold value corresponding to a completely stabilised (consolidated) track, while γ is a parameter that determines the rate of hardening. The parameters of the threshold value are specific for each track site. Thus, in Section 4, these parameters (as well as α_k and β_k) will be calibrated against the field measurements. In each iteration step, up to 10^5 load cycles (corresponding to 3–3.25 MGT of traffic with loaded iron ore trains) are considered. However, an adaptive step length is applied such that a maximum allowed settlement increment $\delta^{\max} = 0.2$ mm per iteration step is allowed. If the increment exceeds δ^{\max} , a linear interpolation is applied.

2.2. Three-dimensional (3D) model

2.2.1. Track model

The second track model is an extensive 3D representation of the superstructure, ballast, and soil in the transition zone [9,26], see Fig. 3 (a). Symmetry conditions, as in the 2D model, are adopted and the simulation of dynamic vehicle–track interaction is carried out using the software ANSYS. Hanging sleepers or voids between slab and foundation are considered using contact elements [26]. This is done to simulate the potential detachment between two adjacent track components during and after the passage of the train. The settings of the applied Normal Penalty Stiffness method [9] were carefully selected to avoid numerical instability. Here, the normal penalty stiffness factor (FKN) was set to 10 to simulate the interaction between sleeper and ballast. Paixão et al. [13] used a similar value in their simulation of contact in ballasted track. To simulate the wheel–rail interaction, FKN = 10^4 was adopted.

In the model, all components are modelled as linear elastic using solid (eight-node brick) elements. The adopted mesh was defined to optimise computational cost and accuracy. Based on a convergence study, the results in terms of calculated displacements and stresses from

different mesh resolutions were compared. The distance between the symmetry plane at the centre of the track model and the opposite boundary (plane yx) on the field side is close to 6 m.

The input data for the superstructure is the same as for the 2D model, cf. Section 2.1 and Table 1. The parameters used for the layers of the trackbed are listed in Table 2, cf. [1,18]. The dynamic analysis of the 3D model is performed using the Newton-Raphson and Newmark methods [9] with a fixed time step of 0.005 s (sampling frequency 200 Hz), while the empirical settlement model was implemented in MATLAB. Rayleigh damping is applied. For the concrete materials and geomaterials, relative damping $\xi = 0.01$ and $\xi = 0.03$ are applied, respectively [9]. The corresponding α and β coefficients were determined based on the specified range of frequencies (5–200 Hz). To avoid spurious wave reflections from the vertical boundaries of the geomaterials (xy plane), viscous dampers are adopted using the Lysmer formulation [29]. This approach has previously been used in the scope of 3D modelling with

Table 2
Parameters of the 3D model.

Substructure		Superstructure	
Ballast	$E = 50$ MPa	Base slab	$E = 30$ GPa
	$\nu = 0.20$		$\nu = 0.20$
	$\rho = 1800$ kg/m ³		$\rho = 2500$ kg/m ³
	$\alpha = 1.84$		$\alpha = 0.61$
Sub-ballast	$\beta = 4.66 \times 10^{-5}$	Top block	$\beta = 1.55 \times 10^{-5}$
	$E = 120$ MPa		$E = 30$ GPa
	$\nu = 0.30$		$\nu = 0.20$
	$\rho = 2100$ kg/m ³		$\rho = 2500$ kg/m ³
Soil layer 1	$\alpha = 1.84$	Block pad	$\alpha = 0.61$
	$\beta = 4.66 \times 10^{-5}$		$\beta = 1.55 \times 10^{-5}$
	$E = 472.5$ MPa		$E = 2.5 \times 10^5$ Pa
	$\nu = 0.25$		$\nu = 0.40$
Soil layer 2	$\rho = 2100$ kg/m ³	Sleepers	$\rho = 2000$ kg/m ³
	$\alpha = 1.84$		$\alpha = 3.06$
	$\beta = 4.66 \times 10^{-5}$		$\beta = 7.76 \times 10^{-5}$
	$E = 800$ MPa		$E = 38$ GPa
	$\nu = 0.25$		$\nu = 0.15$
	$\rho = 2100$ kg/m ³		$\rho = 2500$ kg/m ³
	$\alpha = 1.84$		
	$\beta = 4.66 \times 10^{-5}$		

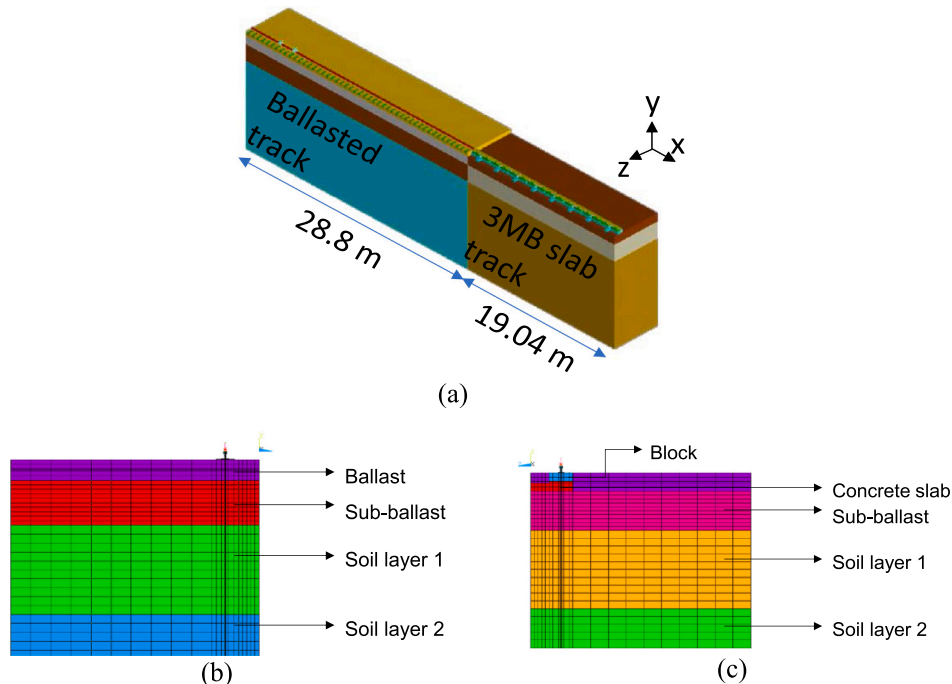


Fig. 3. Sketch of 3D transition zone model: a) General overview of the model, b) cross-section on ballasted track side, c) cross-section on slab track side.

good results, see [29]. On the horizontal boundary at the bottom of the model (xz plane), fixed supports are adopted for both track forms. On the remaining boundaries, viscous dampers (in all directions) are applied for the geomaterials.

2.2.2. Iterative procedure

The 3D model uses an iterative approach. The FE model of vertical dynamic vehicle–track interaction developed in the ANSYS software is integrated with an empirical permanent settlement model to predict the long-term differential settlement along the transition zone [9,29]. Based on the dynamic analysis, the principal stresses, including the deviatoric stresses (q) and mean stresses (p) in the ballast and subgrade layers due to a passing vehicle, are determined. A static analysis is also performed to obtain the initial stresses due to gravity load. These initial stresses are converted to principal, mean (p_{ini}) and deviatoric (q_{ini}), stresses. The permanent deformation is then calculated through the implementation of an empirical equation, cf. Section 2.2.4.

The applied procedure, shown in Fig. 4, covers both the short- and long-term simulations, demonstrating versatility across various models. This process relies on load cycles and stress levels generated by the passing vehicles and the gravity load, with each load cycle corresponding to one vehicle passage. This means that the process is not carried out cycle by cycle (or wheelset by wheelset), but in increments corresponding to a set of cycles (ΔN) assuming that, in this set of cycles, the stress state in the materials remains constant. This interval allows for the progression and eventual stabilisation of permanent deformation (plastic shakedown) [31]. After calculating the distribution of permanent deformation and corresponding track settlement (obtained through the product of the permanent deformation and the vertical length of each finite element), cf. Section 2.2.4, the results are imported into ANSYS again, where the corresponding settlement is applied to each node within the FE model, and the geometry of the track is updated accordingly. In the following iterations, the influence of the modified track geometry on the dynamic performance of the transition zone is assessed, facilitating an examination of the combined effects of stiffness variation and settlement after a specified number of axle passes.

2.2.3. Vertical dynamic vehicle–track interaction

The matrix equation of motion for the coupled vehicle–track model is written as

$$\mathbf{M}\ddot{\mathbf{u}}(t) + \mathbf{C}\dot{\mathbf{u}}(t) + \mathbf{K}\mathbf{u}(t) = \mathbf{F}(t) \quad (10)$$

where \mathbf{F} corresponds to the wheel–rail contact forces that are balanced by $\mathbf{M}\ddot{\mathbf{u}}$ (inertia forces), $\mathbf{C}\dot{\mathbf{u}}$ (damping forces), and $\mathbf{K}\mathbf{u}$ (elastic forces). The displacement vector \mathbf{u}_{n+1} at time $n + 1$ is determined by the assumption:

$$\mathbf{u}_{n+1} = f(\dot{\mathbf{u}}_{n+1}, \ddot{\mathbf{u}}_{n+1}, \mathbf{u}_n, \dot{\mathbf{u}}_n, \ddot{\mathbf{u}}_n, \dots) \quad (11)$$

Based on an assumed constant acceleration in each time interval, the equation of motion is solved using the Newton–Raphson and Newmark method. To obtain an accurate solution, the time step is set depending

on the maximum frequency to be evaluated. The damping matrix is defined based on the Rayleigh damping matrix

$$\mathbf{C} = \alpha\mathbf{M} + \beta\mathbf{K} \quad (12)$$

The parameters α and β are the mass and stiffness proportional damping coefficients, respectively. The absorbing condition proposed in [32], also designated as viscous, is adopted for the treatment of artificial boundaries. The main objective is to eliminate the spurious reflection of a wave when it reaches the boundary. Considering a semi-infinite bar, an interest domain between A and B, and wave propagation in the longitudinal direction from A to B, the main goal is to introduce an absorbing boundary to eliminate the spurious reflection of the wave in the interest domain. Considering the unidirectional character of the problem and a constitutive linear elastic law of the material, it is possible to find the relation between the normal stress induced in any point of a bar and the velocity of that same point. It is given by the expression

$$\sigma_{xx} = \rho C_p \dot{u}_x \quad (13)$$

where C_p is the P wave velocity. In the case of a propagating shear wave, the relationship is similar but now considering the speed of the S wave. Using the Penalty algorithm, the wheel–rail interaction is modelled as a node-to-beam contact allowing for sliding and loss of contact. Contact elements are considered in the sleeper–ballast interface to account for the possible separation of these track elements. The full Newton–Raphson method is used to solve the non-linear equations of the problem, while the Newmark implicit time integration method, with time steps of 0.005 s, is used to solve the dynamic equilibrium equations [9].

2.2.4. Settlement model

For each vehicle model passage in iteration step j ($j = 1, 2, \dots, n_s$), permanent deformation ε_1^p [m/m] in the ballast and subgrade layers is formulated as a function of the principal stresses (three-dimensional stress state), see Eq. (14). The evolution of permanent deformation is only considered for the geomaterials, i.e. ballast, sub-ballast, soil layer 1 and soil layer 2. This model includes the influences of a yielding criterion (through the mechanical properties cohesion and friction angle), the initial stress state and the stresses induced by the passage of the train.

$$\varepsilon_1^p(N_s) = \varepsilon_1^{p0} [1 - e^{-BN}] \left(\frac{\sqrt{p_{am}^2 + q_{am}^2}}{p_a} \right)^a \cdot \frac{1}{m \left(1 + \frac{p_{ini}}{p_{am}} \right) + \frac{s}{p_{am}} - \frac{(q_{ini} + q_{am})}{p_{am}}} \quad (14)$$

Here the parameters ε_1^{p0} , B and a are material constants of the model, m and s are defined by the yielding criterion $q=s+m\cdot p$, N_s is the number of load cycles, p_{ini} and q_{ini} are the initial stress state, p_{am} and q_{am} are the stress levels induced in the subgrade during the passage of the train, while $p_a = 100 \text{ N/m}^2$ is a reference stress with a unit such that the

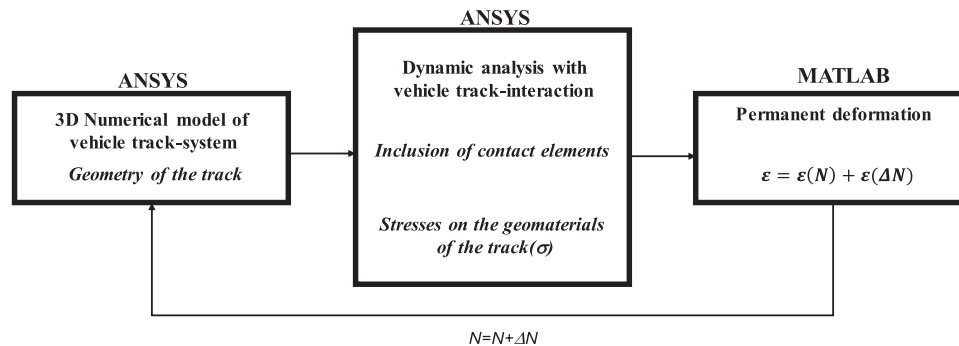


Fig. 4. Iterative procedure to predict differential settlement in a transition zone using the 3D simulation model.

term within the parentheses becomes non-dimensional. Input values will be provided in Section 7.

Next, the accumulated settlement at sleeper i after n_s iteration steps/simulations (corresponding to N_s wheel passages) is calculated by summing the products of element height and calculated permanent deformation over all ballast, sub-ballast and soil foundation elements in the vertical direction. Thus, the accumulated permanent settlement Δ_e is calculated as (in metres)

$$\Delta_e(n_s) = \sum_{e=1}^n \epsilon_{p,e} H_{s,e} \quad (15)$$

where n corresponds to the number of elements that constitute all geo-materials in ballast, sub-ballast, and soil foundations (in the vertical direction), $H_{s,e}$ corresponds to the height of each element e (in metres), $\epsilon_{p,e}$ is the permanent deformation at the centre of each element. With this methodology, it is possible to consider the individual contributions from the ballast, sub-ballast and subgrade layers.

2.3. Vehicle model

The benchmark vehicle model used in this study is a representation of the iron ore freight train operating from the mines in *Kiruna* and *Malmberget* to the ports in *Narvik* (in Norway) and *Luleå*. The train consists of two CoCo locomotives (12 axles) and 68 BoBo wagons (272 axles), resulting in a total of 284 axles distributed over a total length of approximately 750 m. The iron ore wagon used for heavy haul traffic includes one car body and two three-piece bogies, each consisting of a bolster, two side frames and two wheelsets. In [18], it was concluded that each individual wheel passage was not visible in the measured sleeper displacement signal. Instead, each plateau of maximum level corresponded to the passing of four wheels from two adjacent bogies in two adjacent wagons. Thus, in this study, the vehicle model contains two bogies from two adjacent iron ore wagons, cf. Fig. 1(b). The analysis represents the passage of an iron ore train at speed 60 km/h and axle load 31.5 tonnes.

In the 2D model, each bogie is modelled by four dofs, corresponding to the vertical displacements of two wheelsets and the vertical displacement and rotation of the bogie frame. Each primary suspension is represented by a spring with stiffness k_1 and a dashpot with viscous damping c_1 . The weight of half of the car body is accounted for by a static point-load acting at the centroid of the bogie. The parameter values for the vehicle model, see Table 3, were collected from [1]. Each wheel–rail contact is modelled using a non-linear Hertzian contact stiffness.

In the 3D model, the vehicle is modelled with finite elements [29]. The bogies are modelled using rigid beams with distributed mass. As for the 2D model, each wheel is modelled as a rigid unsprung mass, while each primary suspension is modelled using spring and damper elements. Linearised Hertzian wheel–rail contact stiffness $K_H = 1.07 \times 10^3$ kN/mm is assumed.

In the 3D model, the simulation of the passage of the two bogies is performed considering the following procedure: at the start of the analysis, all bogies are stationary. In the subsequent time increments, axle loads and motion characteristics are individually assigned to each bogie, one at a time, in accordance with the train speed and axle configuration, see [9]. With this methodology, the increase in computation time is solely a reflection of the time it takes for the vehicle to travel across the whole track model [9].

Table 3
Parameter values for vehicle model with axle load 32.5 tonnes [1,18].

$k_1 = 30$ MN/m	$c_1 = 70$ kNs/m	$J_w = 100$ kgm ²	$\Delta_{\text{bog}} = 1.74$ m
$J_{\text{bog}} = 730$ kgm ²	$M_w = 1341$ kg	$M_{\text{bog}} = 800$ kg	$\Delta_w = 1.78$ m

3. Field measurements in a transition zone

A setup for condition monitoring of railway track was implemented to assess the influence of traffic load on accumulated differential settlement in a transition zone on the Swedish heavy haul line *Malmbanan* at Gransjö, north of Boden, see [18]. The traffic on *Malmbanan*, a single-track railway line in northern Sweden, is dominated by iron ore freight trains with axle loads up to 32.5 tonnes and speed 60 km/h (70 km/h in tare conditions). The annual traffic load is approximately 15 MGT (Mega Gross Tonnes) with around 850,000 axles in loaded and unloaded iron ore trains. Winters with temperatures down to -40° C, generating ground frost extending deep into the substructure, are followed by frost heaves and floods in the springs and relatively warm summers. As a part of the Horizon 2020 Shift2Rail EU project In2Track3, a demonstrator including 48 m of the 3MB slab track design was constructed at Gransjö. The transition from ballasted track to slab track is used as a benchmark in this study.

Based on fibre Bragg grating (FBG) technology, the instrumentation along the transition comprised four clusters, each with an optical strain gauge array on the rail web in one sleeper bay, and an accelerometer and a displacement transducer on the sleeper. Condition monitoring of the transition zone commenced on the 15th of September 2022 and continued until the 15th of June 2023. The instrumentation for in-situ long-term condition monitoring has been used to provide data for the verification and calibration of the 2D and 3D simulation models.

The long-term settlement of sleepers 5 and 11 from the transition were measured using displacement transducers positioned at each sleeper end. The displacement was measured with respect to a fixed anchor embedded in the ground. Due to space limitations, the transducer was placed horizontally alongside the sleeper and connected via an L-shaped arm mechanism to convert downward vertical movement into horizontal tension/compression on the transducer [18]. Sleeper settlement data has been extracted from times between train passages (unloaded condition). The FBG strain sensors were used to measure axial strain along the rail. By assuming Euler-Bernoulli beam theory for the known rail cross-section with bending stiffness EI , the rail bending moment was determined.

The receptance data involved exciting the rail using an instrumented impact hammer and measuring the track response using accelerometers. Besides the hammer excitation, the track was in unloaded conditions. Accelerations on both ballasted and slab tracks were measured at locations sufficiently far away from the transition zone to mitigate any boundary effects resulting from the change of track form.

4. Calibration of track parameters

As indicated in Section 3, rail receptance (displacement over force) has been measured on both the ballasted track and slab track at the test site. No static preload was applied on the track. In these measurements, the rail was excited in the vertical direction by a hammer either above a rail seat or at the centre in a sleeper bay. Measured point and cross receptances, and their associated coherences, are shown in Fig. 5. Based on the recorded coherences, it is concluded that the quality of the measurements is good above 20 Hz.

For the ballasted side, see Fig. 5(a), three resonance peaks can be observed in the measured receptance at 30, 290 and 950 Hz. The first peak involves a vertical in-phase movement of rail and sleepers, featuring high damping due to the propagation of waves in the ballast and subgrade. The second peak corresponds to an antiphase motion between rail and sleepers on the flexibility of the rail pads. The third peak is the pinned-pinned resonance mode, representing a vertical bending mode with wavelength twice the sleeper span [33].

The measured receptance on the slab side, as depicted in Fig. 5(b), reveals two distinct peaks at about 20 and 90 Hz. The first peak corresponds to the in-phase vibration of rail, top blocks and base slab on the foundation. The second peak is a resonance involving the vibration of rail

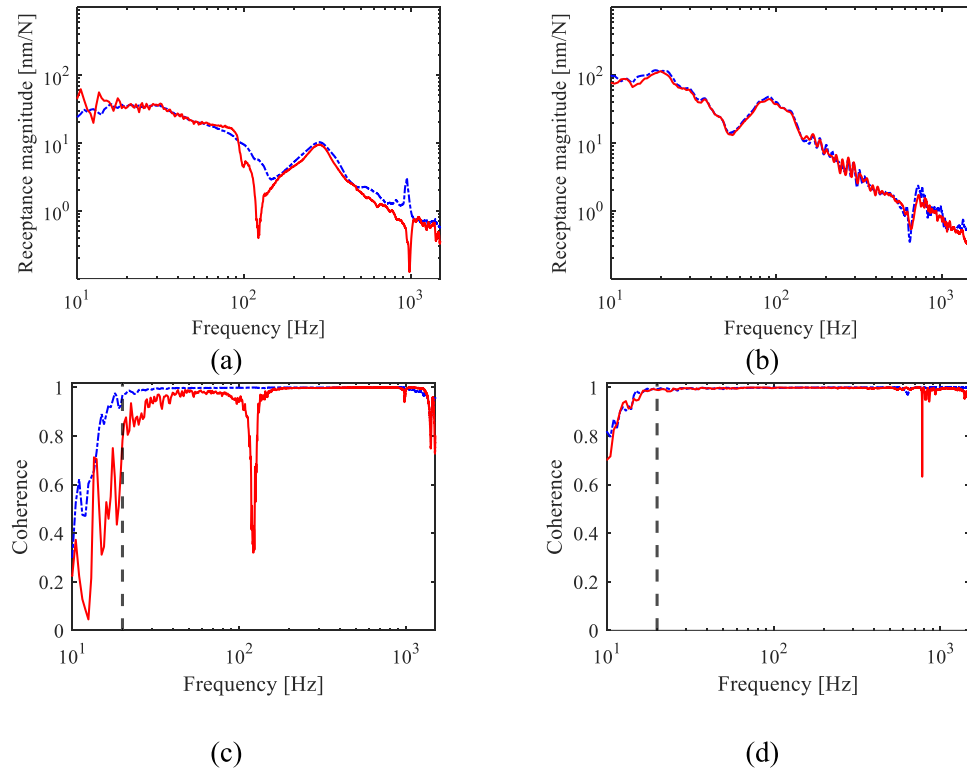


Fig. 5. Magnitudes of measured receptances. Vertical hammer excitation on rail at midspan. Response measured on rail at midspan (point receptance shown using blue lines) or on rail at railseat (cross receptance shown using red lines): a) ballasted track, b) slab track, c) coherence of repeated measurements on ballasted track, d) coherence of repeated measurements on slab track. The vertical-dashed line at 20 Hz denotes the chosen lower frequency limit for the calibration of track parameters.

and top blocks on the rail pads and block pads. The absence of the pinned-pinned resonance might be attributed to the rail fastening on the slab side, which constrains this vibration more than on the ballasted side.

To verify the models of the two track forms and to calibrate their input data, calculated receptances are compared with the corresponding measured receptances. The rail receptance $H_r^t(\omega)$ is determined as

$$H_r^t(\omega) = \frac{x_r^t}{F_r^t}, \quad (16)$$

where x_r^t and F_r^t denote the auto-spectra of the rail displacement and applied force, respectively, while ω is the angular frequency [34].

Based on the measured track receptances, the input parameters for the 2D model indicated with an asterisk in Table 1 have been tuned using the Nelder-Mead optimisation algorithm [35]. The selected lower and upper bounds for each input parameter are listed in Table 4. Note that parameter m_b may represent the vibrating mass of both ballast and part of the subgrade as there is no other considered mass below the 'ballast mass'. The objective function Φ to be minimised was defined as

the quadratic error from the sum of differences \mathbf{e} between the measured and calculated receptances. The error vector \mathbf{e} between the two models is defined as

$$\mathbf{e}(\omega) = \log_{10} H_r^{t, \text{measured}}(\omega) - \log_{10} H_r^{t, \text{model}}(\omega) \quad (17)$$

The use of logarithmic values in the error function is motivated by the large range in receptance in the studied frequency interval. The objective function is written as

$$\Phi = \mathbf{e}^T \mathbf{Q} \mathbf{e} \quad (18)$$

Here \mathbf{Q} is a non-negative weighting matrix (diagonal). To improve accuracy of important features of the track receptance, the elements of \mathbf{Q} corresponding to frequencies at resonances and antiresonances of the measured receptance have been assigned higher weights. To assign higher weights to the static receptance, and to the receptance at the fundamental resonance of the track model, elements in the weighting matrix \mathbf{Q} were set to 4 for the diagonal elements corresponding to frequencies [2 3 33 34 105 106 290 291] Hz. The remaining diagonal

Table 4

Intervals (lower and upper bounds) used in the calibration of track parameters for the 2D model of ballasted track, and output from the optimisation (results). The results are compared with reference values published in the literature.

Parameter (symbol)	Unit	Bounds		Results	Literature
		Lower	Upper		
Rail pad stiffness ($k_{r/s}$)	MN/m	10	1000	110	120[1,21], 65[19], 505 and 738[36,37]
Rail pad damping ($c_{r/s}$)	kNs/m	5	1000	15	40[1], 75[19], 54 and 59[36]
Ballast stiffness (k_b)	MN/m	10	1000	75	100[19], 641 and 767[36]
Ballast damping (c_b)	kNs/m	5	1000	30	58[19], 467 and 460[36]
Ballast mass (m_b)	kg	10	1000	300	250[19]
Subgrade stiffness (k_{sb})	MN/m	10	1000	40	120[19], 603 and 637[36]
Subgrade damping (c_{sb})	kNs/m	5	1000	160	60[19,26], 508 and 797[36]
Ballast shear stiffness (k_w)	MN/m	10	1000	120	78.5[19], 476 and 717[36]
Ballast shear damping (c_w)	kNs/m	5	1000	90	80[19], 173 and 96[36]

elements were set to 1. In the calibration of the parameters, only the magnitudes of the receptances up to 500 Hz were considered, see [38]. Due to the low energy input in the excitation and the low coherence in the measured receptance at frequencies lower than 20 Hz, it is recognised that the measured receptances are not adequate to capture the dynamic properties of the layered soil, cf. Fig. 5(c,d). Instead, the receptance from the 3D model using data from the MASW measurements to represent the properties of the soil have been used as a reference.

The magnitudes of receptance from the different models after calibration are compared with the measured receptances in Fig. 6. For the ballasted track, it is observed that the rail resonance at 290 Hz in the 2D model aligns well with the measured data. The 3D model, with a more detailed representation of the layered foundation, exhibits (at least) two resonances up to 150 Hz. These can also be captured with the seven-parameter representation of the foundation in the 2D model, reaching resonances at 40 and 105 Hz, but here the resonance at about 105 Hz is not visible due to the tuned high damping in the spring-damper element representing the subgrade. A reasonable match between the 2D and 3D models versus the measured data is achieved using the inputs provided in Table 4. For the 2D model, the tuned stiffness value for the combined ballast and USP is 50 MN/m. This stiffness includes the stiffness of the USPs (157 MN/m) and the ballast stiffness without under sleeper pads, which is 75 MN/m. The stiffness and damping of the rail pad on the slab track side was tuned to 30 MN/m and 15 kNs/m, respectively. Inputs for the concrete parts and block pad are specified in Table 2, as per [1,18,39]. The bed modulus on the slab side was tuned to 20 MN/m³. As a side note, based on the 2D model, it has been evaluated that the use of USP leads to a 25 % reduction in stiffness gradient at rail level compared to the case without USP.

5. Interaction between ballast masses in 2D model

The interaction between adjacent ballast masses by implementing the spring k_w and damper c_w in a 2D model has been considered in other track models, see e.g. Oscarsson et al. [36] and Zhai et al. [37]. The range of input data for these two parameters, as well as for the other track parameters as published in various references is vast, see the summary in Table 4. In [19], it was concluded that ballast vibration level in a 2D track model would be overestimated if the shear coupling between ballast masses was not considered, typically leading to a 10 % higher ballast acceleration. In [37], the calculated ballast acceleration using a stiff shear coupling was 16 % lower than measured data.

The influence of a wide range of stiffnesses k_w on FRFs for rail displacement (point receptance) and ballast mass displacement (cross receptance) when subjected to a harmonic load applied on the rail, and time histories of sleeper displacement and sleeper–ballast contact force for a vehicle model passage is illustrated in Fig. 7(a–d). Here, the damping c_w was scaled in linear proportion to k_w using the factor 0.001, cf. [40]. In Fig. 7(a), it is observed that the calculated rail receptance for

lower values of k_w has three distinct peaks within the studied frequency range, at about 40, 105 and 290 Hz. In Fig. 7(b), it is shown that a higher k_w leads to a lower cross receptance for the ballast mass that is located directly below the applied load. The influence of k_w is only significant up to about 400 Hz. It was observed (not shown here) that the influence of different values of k_w on the time histories of wheel–rail contact force and rail bending moment is negligible. As expected, larger values of k_w lead to smaller sleeper displacements because of the stiffer track model and the stronger interaction between sleepers, see Fig. 7(c). Interestingly, the influence of k_w on sleeper–ballast force is relatively small as the smaller relative sleeper–ballast displacement is compensated by the higher stiffness leading to that the product of stiffness and relative displacement is similar, see Fig. 7(d).

The influence of k_w on the force transmissibility, i.e. the ratio between the sleeper–ballast contact force and a unit harmonic load applied on the rail, is shown in Fig. 7(e,f). For stationary harmonic vibration, the complex-valued amplitude of the sleeper–ballast force is calculated as

$$\hat{F}_{s/b} = (k_b + i\omega c_b)(\hat{x}_{\text{sleeper}} - \hat{x}_b) \quad (19)$$

where the hat symbol indicates amplitude. In this example, the load was applied on the rail above sleeper 25, and the force transmissibility was calculated for the ballast springs below sleepers 23, 24, 25, 26 and 27. The magnitude of the force transmissibility for the cases $k_w = 0$ and 120 MN/m are compared in Fig. 7(e,f). For both cases, there is a local maximum in the force transmissibility at about 40 Hz. The static distribution (at 0 Hz) of the force transmissibility between adjacent sleepers is indicated by the numbers next to the vertical axis. For example, in the case of zero shear stiffness, the applied load on the rail above sleeper 25 is principally supported by five sleepers with 31 % on sleeper 25, 23 % on each of the sleepers 24 % and 26 %, and 11 % on each of the sleepers 23 and 27 (total of 99 %). For zero shear stiffness, it is observed that the load is distributed more evenly among the sleepers, and the track flexibility at rail level is higher, cf. Fig. 7(a). Conversely, when the shear stiffness is 120 kN/mm, a larger proportion of the applied load is transmitted to the sleeper directly below the applied load. This is because, as the support system modulus is increased a shorter length of the rail is subjected to bending leading to a reduced distribution of load [41]. The distribution of vertical load is in good agreement with results from field measurements in ballasted track as reported in [18].

6. Short-term dynamic response

To further verify the 2D and 3D track models presented in Section 2, calculated short-term dynamic responses are compared with measured data. One-way traffic of a loaded iron ore train at speed 60 km/h in the direction from the stiffer ballasted track to the softer slab track is considered.

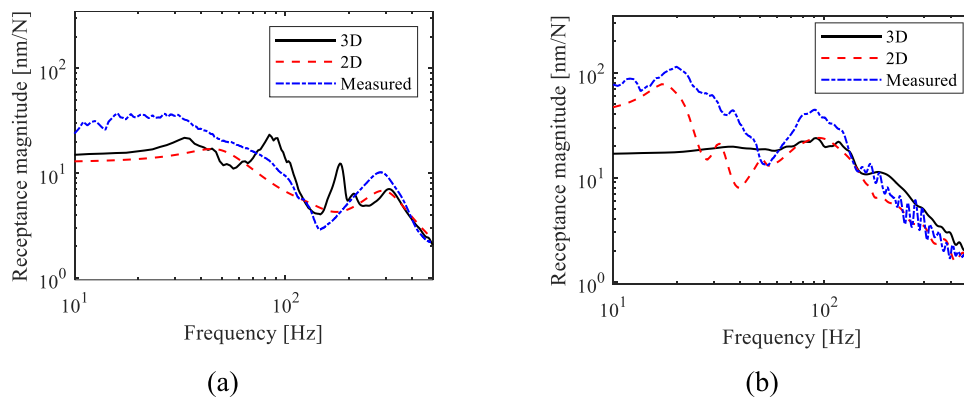


Fig. 6. Comparison of measured and calculated rail receptances: a) ballasted track, b) slab track.

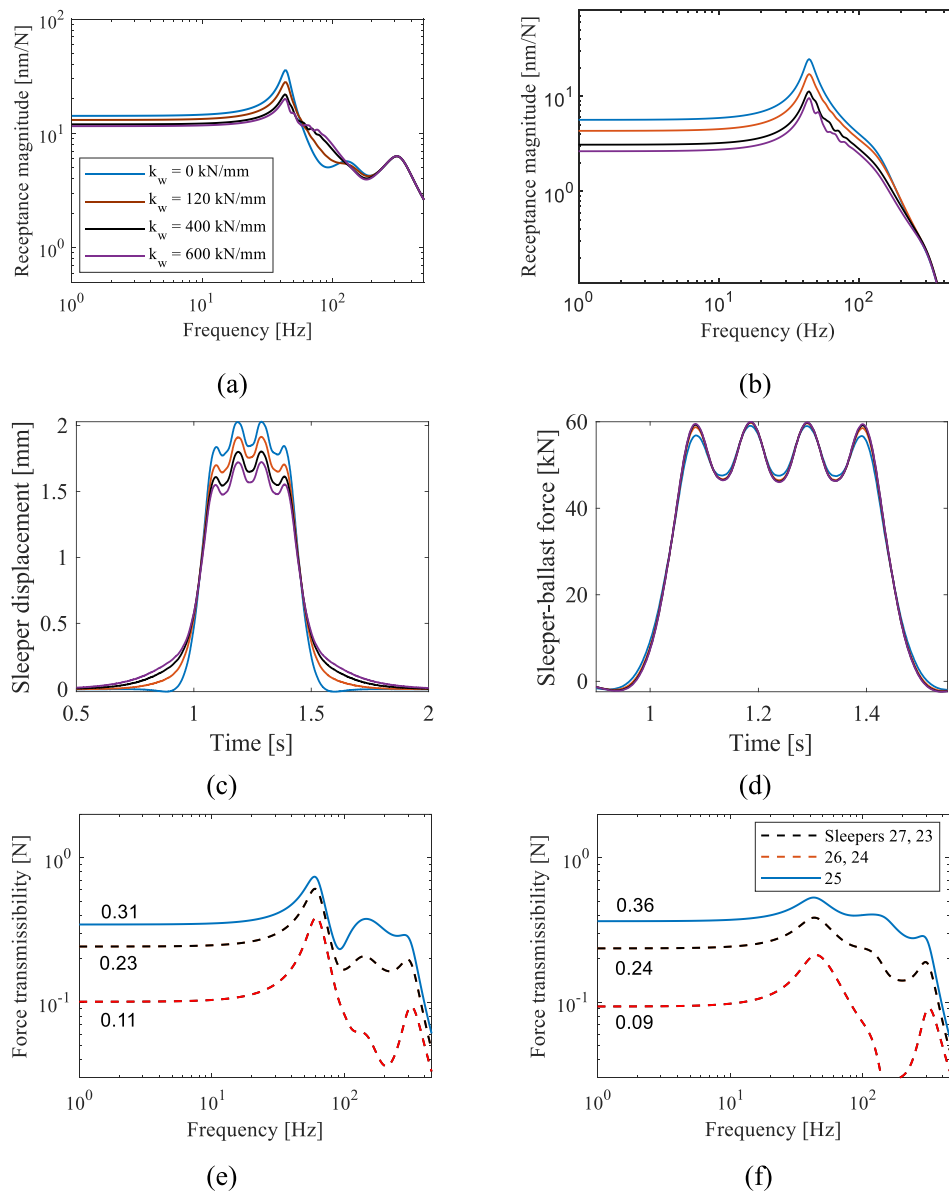


Fig. 7. Influence of ballast shear stiffness k_w on various track responses: a) point receptance on the rail above sleeper 25, b) cross receptance on the ballast mass below sleeper 25, c) time history of displacement for sleeper 25, d) time history of sleeper-ballast contact force acting on sleeper 25, e) transmissibility from a load applied on the rail above sleeper 25 to sleeper-ballast contact forces acting on adjacent sleepers for $k_w = 0$ kN/mm, f) corresponding force transmissibility for $k_w = 120$ kN/mm. The same legend holds for Fig. 7(a-d), and the same legend holds for Fig. 7(e and f).

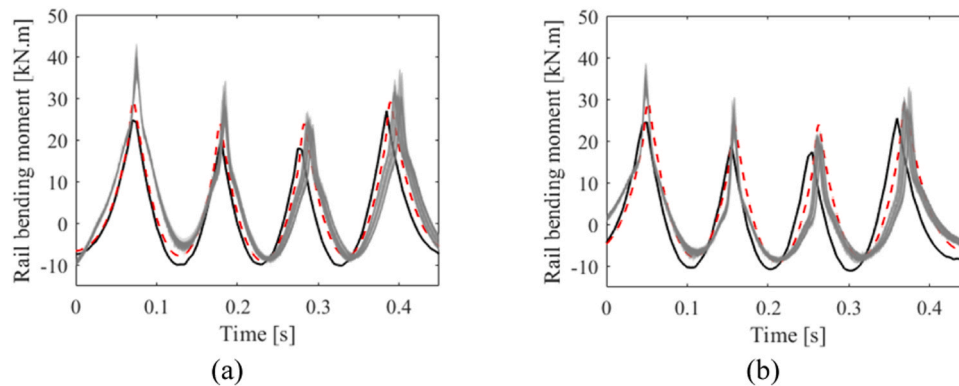


Fig. 8. Measured and simulated time histories of rail bending moment above sleepers (a) 5 and (b) 11. Measurement from 2022-10-13, 7 days after construction of the transition zone. Black solid lines, red dashed lines, and shaded area correspond to 3D, 2D models, and measured rail bending moment, respectively.

6.1. Rail bending moment

Time histories of rail bending moment above sleepers 5 and 11 from the transition have been simulated using the calibrated 2D and 3D FE models. In Fig. 8, these are compared with the corresponding measured rail bending moments [18]. In the measurements, the bending strain due to 68 passing iron ore wagons with an uncertain distribution of axle loads was recorded. The response due to the pass-by of two bogies in two adjacent wagons is illustrated in Fig. 8. The variability in measured bending strains between passing wagons is indicated by the shaded area. For both models, there is good agreement between the measured and calculated signatures (time histories) of the rail bending moment. The maxima of the measured rail bending moments are higher indicating a softer track (including voided sleepers, see Section 6.2) in the field compared to in the models.

6.2. Sleeper displacement

Time histories of measured and simulated sleeper displacements due to the pass-by of two bogies in two adjacent wagons are compared in Fig. 9. The measurements were taken from sleepers 5 and 11 from the transition. Similarly, the variability in measured sleeper displacement is indicated by the shaded area, accounting for all wagon passages in one train passage. According to the measurements, sleepers 5 and 11 were subjected to a larger range of displacements indicating voids between sleeper and ballast of 1.15 mm and 1.60 mm, respectively. Since the support conditions in the virgin track models were assumed to be uniform, these voids have been subtracted from the measured data in Fig. 9. Good agreement between measured and simulated signatures of sleeper displacement is observed, and the magnitudes of the calculated sleeper displacements obtained from both models are found to be essentially consistent with the measured data.

6.3. Sleeper-ballast contact force

Time histories of simulated sleeper-ballast contact forces from the 2D and 3D models due to the pass-by of two bogies in two adjacent wagons are compared. Unfortunately, there is no corresponding measured force to compare with. In Fig. 10, the sleeper-ballast contact force for sleeper 5 and 11 generated due to passage of four wheels from two bogies in two adjacent iron ore wagons is shown. Good agreement between the two models is observed. In the 2D model, for each wheel passage and each sleeper, the maximum sleeper-ballast contact force is identified and used as input in the empirical settlement model, cf. Section 2.1.4.

7. Long-term settlement

As described above, the aim of this study is to compare two models for the prediction of long-term differential settlement in a transition zone between ballasted track and slab track. Initially, the specific input parameters in each empirical settlement model were tuned by comparing the calculated settlement with settlements measured in the transition zone at Gransjö, see [18]. For a traffic load of 8 MGT, the measured long-term evolution of accumulated settlement for sleepers 5 and 11 from the transition is shown in Fig. 11, see the dashed blue and black lines. After an initial phase of very rapid settlement development up to a traffic load of about 1 MGT, the permanent deformation rate decreases significantly, a phenomenon referred to as shakedown [29].

For the tuning of the 2D settlement model, the time history of the sleeper-ballast contact force was calculated at a sleeper away from the transition zone, where it was assumed that the evolving differential settlement compared to adjacent sleepers is negligible. Based on the simplification of remaining constant up to an accumulated traffic load of 12 MGT, the maximum sleeper-ballast contact force was used as input in Eqs. (7) and (9). By applying the iterative approach illustrated in the lower (boxed in) part of Fig. 2, the settings of input parameters α_1 , β_1 , $F_{th,0}$, $F_{th,\infty}$ and γ were tuned such that the trend of the evolving settlement agreed with the measured settlement for sleeper 11, see Fig. 11. Input data for the calibrated parameters are listed in Table 5.

Similarly, for the 3D model, one short-term analysis was conducted to extract the stresses in all directions for the different layers (ballast, sub-ballast, soil layers 1 and 2). These stresses were exported to MATLAB to calculate the principal stresses, deviatoric stresses q and mean stresses p . Additionally, a static analysis was performed to obtain the initial stresses due to gravity load on the track structure. These were converted to mean p_{ini} and deviatoric q_{ini} stresses. The parameters m and s in Eq. (14) were determined based on input for the cohesion and friction angle of ballast, sub ballast, soil layers 1 and 2 taken from [9, 29]. The parameters $ep1$, B and a were also taken from [9, 29]. Input data for the calibrated parameters are listed in Table 5. It is observed that the tuned curve is in good agreement with the long-term trend for the measured settlement. As described in Section 2.2.2, the settlement curve can be applied in an iterative procedure to predict the differential settlement within the transition zone. In that case, the calculated permanent track displacement after a certain number of load cycles is applied to each node within the FE model, and the geometry of the track is updated accordingly before a new short-term analysis of the dynamic loading is carried out in ANSYS, etc. However, this procedure has not been carried out since the estimated time per iteration step (short-term analysis) for this particular transition zone model would be in the order of 4 days due to the extensive length of the model and the large number of degrees of freedom.

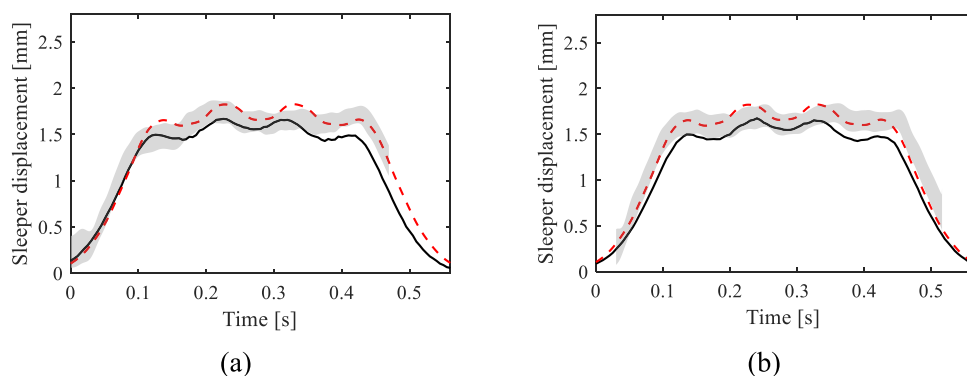


Fig. 9. Measured and simulated time histories of sleeper displacement: (a) sleeper 5, (b) sleeper 11. Measurement from 2022–10–14, 8 days after construction of the transition zone. For the 3D case with the flexible sleeper model, the displacement was calculated at railseat. The voided contribution to the displacements has been subtracted from the measured data (1.60 mm for sleeper 5 and 1.15 mm for sleeper 11). Black solid lines, red dashed lines, and shaded area correspond to 3D, 2D models, and measured sleeper displacement, respectively.

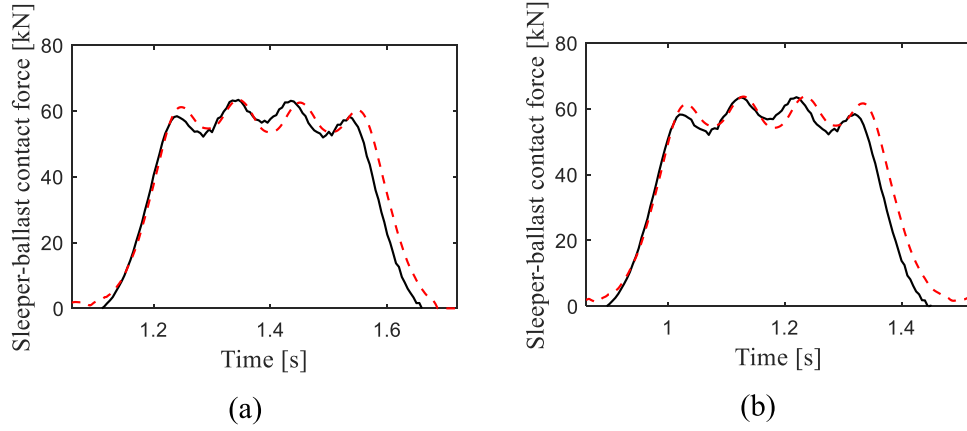
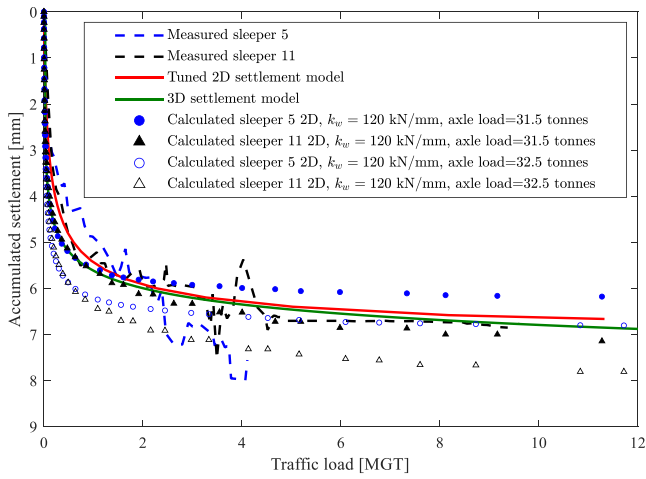
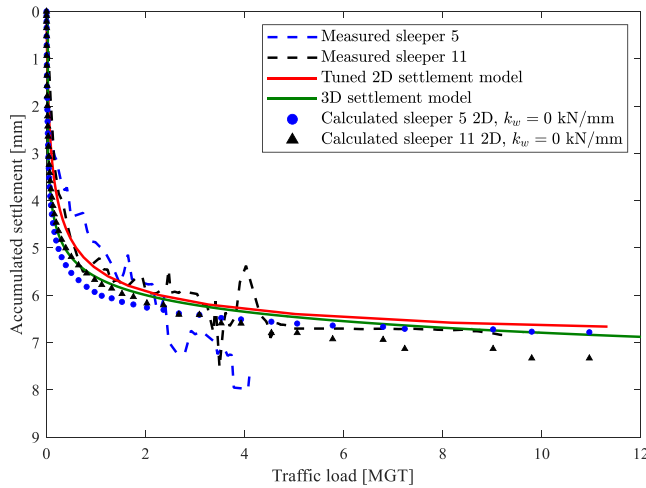


Fig. 10. Calculated sleeper-ballast contact forces using the 2D and 3D models: (a) sleeper 5 and (b) sleeper 11. Black solid lines and red dashed lines correspond to 3D and 2D models, respectively.



(a)



(b)

Fig. 11. Comparison of measured (copied from [18]) and calculated accumulated settlement for sleepers 5 and 11: (a) $k_w = 120$ kN/mm in 2D model, (b) $k_w = 0$ kN/mm in 2D model. The numbers of iterations with the 2D model when $k_w = 120$ kN/mm and $k_w = 0$ kN/mm were 46 and 52, respectively. The number of iterations with the 3D model was 1. See Table 5 for input data to tuned settlement models.

Table 5

Tuned parameter values for settlement models.

2D model		3D model				
Parameter [unit]	Value	Parameter [unit]	Value	Value	Value	Value
γ [1/mm]	0.11	m	2.057	1.976	1.636	1.331
$F_{th, \infty}$ [kN]	90	s [Pa]	1.726	1.779	1.950	2.049
$F_{th, 0}$ [kN]	35	ϵ_1^{p0}	0.004	0.00093	0.00093	0.00093
β_1	2.8	B	0.2	0.2	0.2	0.2
α_1 [mm/ 10^5]	0.02	a	0.65	0.65	0.65	0.65

Fig. 11(a) compares the measured and calculated accumulated settlements for sleepers 5 and 11 up to an accumulated traffic load of 12 MGT. In the virgin state of both transition zone models, uniform support conditions and no voided sleepers were assumed. For the 2D model, 46 iterations (the result after each iteration is marked with a dot) with subsequently updated state-dependent track support conditions and settings in the settlement model, cf. Fig. 2, were completed in about 5 days. The maximum settlement increment per iteration step was set to 0.2 mm leading to very small steps in traffic load up to about 2 MGT. Due to the stiffness gradient and the evolving misalignment in rail level, there is a dynamic excitation of the vehicle-track system leading to a local maximum in settlement around sleepers 4 – 11 (at 2 – 6 m from the transition) [42]. This will create a loop of increasing dynamic excitation of the system leading to higher sleeper-ballast contact forces, further settlement, etc. Note that the development of voided sleepers near the transition leads to a redistribution of load to the adjacent sleepers farther away from the transition. This will generate higher settlement at these sleepers, and eventually a small shift in the location of the local maximum in longitudinal level, cf. the larger calculated settlement for sleeper 11 than for sleeper 5. Due to the increase (hardening) of the settlement threshold value with increasing accumulated settlement, there is eventually a stabilisation (slowing down) of the settlement.

In Fig. 11(b), the influence of excluding the shear coupling ($k_w = 0$) between adjacent ballast masses in the 2D track model on the predicted long-term sleeper settlement is studied. As can be seen from Fig. 7(d), the sleeper-ballast force is smaller for the case when $k_w = 0$, leading to a smaller increment in settlement per iteration step. Thus, more iterations were required to reach shakedown in the accumulated settlement curve, cf. Fig. 11(b). The number of iterations in this case was 52. However, higher k_w leads to a larger difference in settlement between sleepers resulting in more differential settlement, cf. Fig. 11(a). To further demonstrate the 2D model, the axle load was increased from 31.5 tonnes

to 32.5 tonnes. As expected, this leads to an increase in long-term settlement, see Fig. 11(a).

8. Concluding remarks

In this paper, two models of vertical dynamic vehicle–track interaction in a transition zone between a ballasted track and a 3MB slab track have been calibrated and validated against rail receptances, rail bending moments and sleeper displacements measured in the field. The first model is a reduced-order 2D representation of the transition zone between ballasted track and 3MB slab track, incorporating the interaction between adjacent sleepers through the ground via a discretised seven-parameter mass-spring-damper model. The second model is an extensive 3D FEM-PML representation of the transition zone, where superstructure, ballast and layered soil are represented by solid finite elements. The computational cost for the 2D model is significantly lower than for the 3D model at the expense of a very much more simplified representation of the foundation.

Both models have been employed to simulate the passage of an iron ore freight vehicle with axle loads 31.5 tonnes through the transition zone at 60 km/h. Good agreement was observed between the measured rail bending moments and sleeper displacements and the corresponding dynamic responses calculated with the 2D and 3D models, with the simulation time being approximately 25 times shorter for the 2D model.

Based on measured long-term sleeper settlements in the transition, two alternative empirical settlement models have been tuned successfully. To demonstrate one numerical approach to predict long-term differential settlement, the iterative procedure used with the 2D model has been applied for a traffic load of 12 MGT. Based on in the order of 50 iterations, it was shown that the predicted settlement was in good agreement with the in-situ measurements. For a further verification of the 2D model, it was shown that an increase in axle load resulted in an increase in the long-term settlement. It is argued that both the 2D and 3D models are capable of successfully representing the short-term and long-term response of the vehicle–track system in the transition zone. Therefore, the choice between these models depends on the specific requirements of the analysis, including the desired level of accuracy and available computational capabilities.

Author Statement

We are pleased to submit our manuscript entitled “**Benchmark of calibrated 2D and 3D track models for simulation of differential settlement in a transition zone using field measurement data**”, to be considered for publication in the journal of Engineering Structures. This paper calibrates and validates the 2D and 3D models for time-domain simulation of vertical dynamic vehicle–track interaction, as well as the applied empirical equations to predict differential long-term settlement of sleepers in a transition zone.

This manuscript has not been previously published and is not under consideration in the same or substantially similar form in any other peer-reviewed media. A preliminary and very much shorter version of the manuscript was presented in Nasrollahi K, Ramos A, Nielsen J, Dijkstra J and Ekh M. Calibration of 2D and 3D track models for simulation of vehicle–track interaction and differential settlement in transition zones using field measurement data. proceedings of the 28th IAVSD International Symposium on Dynamics of Vehicles on Roads and Tracks, IAVSD2023, August 17–21, 2023, Ottawa, Canada.

CRediT authorship contribution statement

Kourosh Nasrollahi: Writing – original draft, Visualization, Validation, Software, Methodology, Investigation, Formal analysis, Data curation, Conceptualization. **Ana Ramos:** Writing – review & editing, Investigation, Formal analysis. **Jens C.O. Nielsen:** Writing – review & editing, Supervision, Project administration, Methodology, Funding

acquisition, Conceptualization. **Jelke Dijkstra:** Writing – review & editing, Supervision, Project administration, Methodology, Conceptualization. **Magnus Ekh:** Writing – review & editing, Supervision, Methodology, Conceptualization.

Declaration of Competing Interest

The authors declare that they have no known competing financial interests or personal relationships that could have appeared to influence the work reported in this paper.

Data availability

Data will be made available on request.

Acknowledgement

The current study is part of the ongoing activities in CHARMEC – Chalmers Railway Mechanics (www.chalmers.se/charmec). Parts of the study have been funded from the European Union’s Horizon 2020 research and innovation programme in the In2Track3 project under grant agreement 101012456, and from the Europe’s Rail Flagship Project IAM4RAIL– Holistic under grant agreement 101101966. This work was also partly financed by FCT/MCTES through national funds (PIDDAC) under the R&D Unit CONSTRUCT – Institute of R&D in Structures and Construction, reference UIDB/04708/2020. Discussions with Mr. Carlos Hermosilla, and Drs. Astrid Pieringer and Jannik Theyssen are gratefully acknowledged. Parts of the simulations were performed using resources at Chalmers Centre for Computational Science and Engineering (C3SE) provided by the Swedish National Infrastructures for Computing (SNIC).

References

- [1] Nasrollahi K, Nielsen JCO, Aggestam E, Dijkstra J, Ekh M. Prediction of long-term differential track settlement in a transition zone using an iterative approach. *Eng Struct* 2023;283:115830.
- [2] Sakhare A, Punetha P, Meena NK, Nimbalkar S, Dodagoudar GR. Dynamic behaviour of integral abutment bridge transition under moving train loads. *Transp Geotech* 2023;40:100989.
- [3] Varandas JN, Hölscher P, Silva MAG. Dynamic behaviour of railway tracks on transition zones. *Comput Struct* 2011;89:1468–79.
- [4] Coelho B, Hölscher P, Priest J, Powrie W, Barends F. An assessment of transition zone performance. *Proc Inst Mech Eng, Part F* 2011;225:129–39.
- [5] Fortunato E, Paixão A, Calçada R. Railway track transition zones: design, construction, monitoring, and numerical modelling. *Int J Railw Technol* 2013;2:33–58.
- [6] Wang H, Markine V. Dynamic behaviour of the track in transition zones considering the differential settlement. *J Sound Vib* 2019;459:114863.
- [7] Jain A, Marykovskiy Y, Metrikine AV, van Dalen KN. Quantifying the impact of stiffness distributions on the dynamic behaviour of railway transition zones. *Transp Geotech* 2024;45:101211.
- [8] Indraratna B, Babar Sajjad M, Ngo T, Gomes Correia A, Kelly R. Improved performance of ballasted tracks at transition zones: a review of experimental and modelling approaches. *Transp Geotech* 2019;21:100260.
- [9] Ramos A, Gomes Correia A, Calçada R, Connolly DP. Ballastless railway track transition zones: an embankment to tunnel analysis. *Transp Geotech* 2022;100728.
- [10] Wang H, Markine V. Modelling of the long-term behaviour of transition zones: prediction of track settlement. *Eng Struct* 2018;156:294–304.
- [11] Shan Y, Zhou S, Zhou H, Wang B, Zhao Z, Shu Y, et al. Iterative method for predicting uneven settlement caused by high-speed train loads in transition-zone subgrade. *Transp Res Rec* 2017;2607:7–14.
- [12] Shan Y, Zhou S, Wang B, Ho CL. Differential settlement prediction of ballasted tracks in bridge–embankment transition zones. *J Geotech Geoenviron Eng* 2020;146:1–18.
- [13] Paixão A, Fortunato E, Calçada R. Transition zones to railway bridges: track measurements and numerical modelling. *Eng Struct* 2014;80:435–43.
- [14] Aggestam E, Nielsen JCO. Multi-objective optimisation of transition zones between slab track and ballasted track using a genetic algorithm. *J Sound Vib* 2019;446:91–112.
- [15] Grossoni I, Hawksbee S, Jorge P, Bezin Y, Magalhaes H. Prediction of track settlement at high-speed railway transitions between embankment and bridge in the proximity of a turnout. *Transp Geotech* 2022;37:100879.
- [16] Dahlberg T. Railway track stiffness variations - consequences and countermeasures. *Int J Civ Eng* 2010;8:1–12.

- [17] Sañudo R, Dell'Olio L, Casado JA, Carrascal IA, Diego S. Track transitions in railways: a review. *Constr Build Mater* 2016;112:140–57.
- [18] Nasrollahi K, Dijkstra J, Nielsen JCO. Towards real-time condition monitoring of a transition zone in a railway structure using fibre Bragg grating sensors. *Transp Geotech* 2024;44:101166.
- [19] Zhai WM, Wang KY, Lin JH. Modelling and experiment of railway ballast vibrations. *J Sound Vib* 2004;270:673–83.
- [20] Esveld C. *Modern railway track*, MRT-productions, Zaltbommel. 2001.
- [21] Theyssen JS, Aggestam E, Zhu S, Nielsen JCO, Pieringer A, Kropp W. Calibration and validation of the dynamic response of two slab track models using data from a full-scale test rig. *Eng Struct* 2021;234:111980.
- [22] Germonpré M, Nielsen JCO, Degrande G, Lombaert G. Contributions of longitudinal track unevenness and track stiffness variation to railway induced vibration. *J Sound Vib* 2018;437:292–307.
- [23] Dahlberg T. Some railroad settlement models - a critical review. *Proc Inst Mech Eng, Part F* 2001;215:289–300.
- [24] Abadi T, Le Pen L, Zervos A, Powrie W. A review and evaluation of ballast settlement models using results from the Southampton railway testing facility (SRTF). *Procedia Eng* 2016;143:999–1006.
- [25] Sato Y. Japanese studies on deterioration of ballasted track. *Veh Syst Dyn* 1995;24:197–208.
- [26] Ognibene G., Powrie W., Le Pen L, Harkness J. Analysis of a bridge approach: Long-term behaviour from short-term response. In: *Proceedings of the 15th Railway Engineering Conference*, Edinburgh, UK, 2019, 1–15.
- [27] Punetha P, Nimbalkar S, Khabbaz S. Simplified geotechnical rheological model for simulating viscoelasto-plastic response of ballasted railway substructure. *Int J Numer Anal Methods Geomech* 2021;45(14):2019–47.
- [28] Suiker ASJ, De Borst R. A numerical model for the cyclic deterioration of railway tracks. *Int J Numer Methods Eng* 2003;57(4):441–70.
- [29] Ramos A, Gomes Correia A, Calçada R, Alves Costa P, Esen A, Woodward PK. Influence of track foundation on the performance of ballast and concrete slab tracks under cyclic loading: physical modelling and numerical model calibration. *Constr Build Mater* 2021;277:122245.
- [30] Nielsen JCO, Li X. Railway track geometry degradation due to differential settlement of ballast/subgrade – numerical prediction by an iterative procedure. *J Sound Vib* 2018;412:441–56.
- [31] Werkmeister S, Dawson AR, Wellner F. Permanent deformation behavior of granular materials and the shakedown concept. *Transp Res Rec* 2001;1757:75–81.
- [32] Lysmer J, Kuhlemeyer L. Finite dynamic model for infinite media. *J Eng Mech Div* 1969;95.
- [33] Knothe K, Wu Y. Receptance behaviour of railway track and subgrade. *Arch Appl Mech* 1998;68:457–70.
- [34] Thompson D. *Track vibration*. Railway Noise and Vibration. Elsevier.; 2009. p. 29–95.
- [35] Nelder JA, Mead R. A simplex method for function minimization. *Computer* 1965;7:308–13.
- [36] Oscarson J, Dahlberg T. Dynamic train/track/ballast interaction - computer models and full-scale experiments. *Veh Syst Dyn* 1998;29:73–84.
- [37] Zhai W, Wang K, Cai C. Fundamentals of vehicle-track coupled dynamics. *Veh Syst Dyn* 2009;47:1349–76.
- [38] Johansson A, Nielsen JCO, Bolmsvik R, Karlström A, Lundén R. Under sleeper pads -Influence on dynamic train-track interaction. *Wear* 2008;265:1479–87.
- [39] Morales-Gamiz FJ. Design requirements, concepts, and prototype test results for new system of ballastless system (3MB slab track). *Capacit rail; Deliv* 2017;11:3.
- [40] Nielsen JCO. High-frequency vertical wheel-rail contact forces - validation of a prediction model by field testing. *Wear* 2008;265:1465–71.
- [41] Powrie W. *A guide to track stiffness*. University of Southampton Department of Civil and Environmental Engineering; 2016.
- [42] Nicks J.E. *The bump at the end of the railway bridge*. Texas, United States: Texas A&M University; 2009. PhD Thesis.